ADVANCED FUNCTIONAL MATERIALS
www.afm-journal.de

Ultrafast Fabrication of Covalently Cross-linked Multifunctional Graphene Oxide Monoliths

Wubo Wan, Lingli Li, Zongbin Zhao, Han Hu, Xiaojuan Hao, David A. Winkler, Lingcong Xi, Timothy C. Hughes, and Jieshan Qiu**

Stable graphene oxide monoliths (GOMs) have been fabricated by exploiting epoxy groups on the surface of graphene oxide (GO) in a ring opening reaction with amine groups of poly(oxypropylene) diamines (D_{400}). This method can rapidly form covalently bonded GOM with D_{400} within 60 s. FTIR and XPS analyses confirm the formation of covalent C-N bonds. Investigation of the GOM formation mechanism reveals that the interaction of GO with a diamine cross-linker can result in 3 different GO assemblies depending on the ratio of D_{400} to GO, which have been proven both by experiment and molecular dynamics calculations. Moreover, XRD results indicate that the interspacial distance between GO sheets can be tuned by varying the diamine chain length and concentration. We demonstrate that the resulting GOM can be moulded into various shapes and behaves like an elastic hydrogel. The fabricated GOM is non-cyctotoxic to L929 cell lines indicating a potential for biomedical applications. It could also be readily converted to graphene monolith upon thermal treatment. This new rapid and facile method to prepare covalently cross-linked GOM may open the door to the synthesis and application of next generation multifunctional 3D graphene structures.

1. Introduction

Graphene is a remarkable material that is made of single layer of carbon atoms.[1] Its unique physical and chemical properties make graphene a promising material for a wide range of applications such as flexible electronics,[2] catalyst supports,[3] and energy related applications.[4] The self-assembly of individual graphene sheets into a macro graphene monolith is critical to accomplish many of the aforementioned applications.[5] Graphene oxide (GO) is the oxidized form of graphene that has abundant highly reactive oxygen-containing groups on its flat surface, which makes it an ideal precursor to form versatile macro graphene-based structures. Multifunctional two-dimensional (2D) graphene[6] and GO[7] films were initially synthesized by vacuum induced self-assembly methods using GO as a precursor. These conductive and mechanically strong graphene films have paved their way into applications such as flexible electrodes[8,9] and electrochemical sensors.[10,11] Recently, three-dimensional (3D) graphene/GO architectures have attracted a lot of attention due to their low density[12] and high surface area,[13] as well as their unique mechanical[14] and electrical properties.[13] Wang et al. initially reported a hydrothermal method to produce a 3D graphene monolith promoted by different noble metals.[5] Then Worsley et al. introduced a sol–gel process to produce a similar 3D macro assembly of graphene sheets.[13] The direct synthesis of a graphene monolith was first reported by Shi et al. using a one-step hydrothermal procedure without using any other chemical agents.[15] Following this, many different approaches, including the use of small organic molecules,[16,17] metal ions,[18,19] and polymers[20,21] have been employed to facilitate the formation of a 3D graphene monolithic structure through non-covalent chemical interactions. The formation of a macro assembled graphene structure has also been achieved through the chemical reduction of GO by various reducing agents.[14,22] However, most of the previous methods required high temperature and/or long reaction times to form the 3D GO geometries. Most studies to date have been focused on the structural, mechanical, and/or electronic properties of the synthesized graphene monoliths, whilst the mechanism behind the formation of these graphene based structures is not yet well understood. Moreover, many of the previously reported methods attributed the formation of a 3D geometry to non-covalent interactions, such as π–π stacking,[15,23] hydrogen bonding,[24] or electrostatic interactions.[21] However, there have been very few studies of covalently bonded 3D GO structures[25,26] and the mechanism(s)

W. B. Wan, Prof. Z. B. Zhao, H. Hu, L. Xi, Prof. J. S. Qiu
Carbon Research Laboratory
Liaoning Key Lab for Energy Materials
and Chemical Engineering
State Key Lab of Fine Chemicals
School of Chemical Engineering
Dalian University of Technology
Dalian 116024, P. R China
E-mail: jqiu@dlut.edu.cn
W. B. Wan, L. L. Li, X. J. Hao, D. A. Winkler, T. C. Hughes
Materials Science and Engineering
Commonwealth Scientific and Industrial
Research Organization (CSIRO)
Clayton, VIC 3168, Australia
E-mail: tim.hughes@csiro.au
L. L. Li
School of Optometry & Ophthalmology
Wenzhou Medical University
Wenzhou 325000, P. R China
D. A. Winkler
Monash Institute of Pharmaceuticals Sciences
Parkville 3052, Australia

DOI: 10.1002/adfm.201303815

behind their formation have not been fully investigated. In order to explore the practical applications of this new material, an effective and simple method to fabricate the 3D graphene based monoliths is needed.

In this report, we investigated a rapid and facile cross-linking methodology to fabricate 3D multifunctional graphene oxide monolithic (GOM) structures by covalent chemical bonding. The developed method can form cross-linked GOM within 1 min under mild conditions, in the presence of a traditional epoxy curing agent, D_{400}, as a cross-linker. D_{400} is a polyoxypropylene diamine with two active primary amine groups located on secondary carbon atoms at each end of an aliphatic polyether chain (Scheme S1), which makes it a suitable binder to stitch two or more GO sheets together. It was revealed that the C–N bond formation is the driving force to form the GOM. Investigation of the mechanism for the formation of GOM strongly suggests that the intercalations of D_{400} with GO have three different conformations, which can result in different GO assemblies. Furthermore, the fabricated GOM demonstrated shape memory behavior as it can recover to the original dimensions when it is re-hydrated. This ultrafast cross-link method has the advantage of simplicity and scalability, which can provide an alternative rapid route to the fabrication of versatile graphene based macrostructures with tunable intercalation distances.

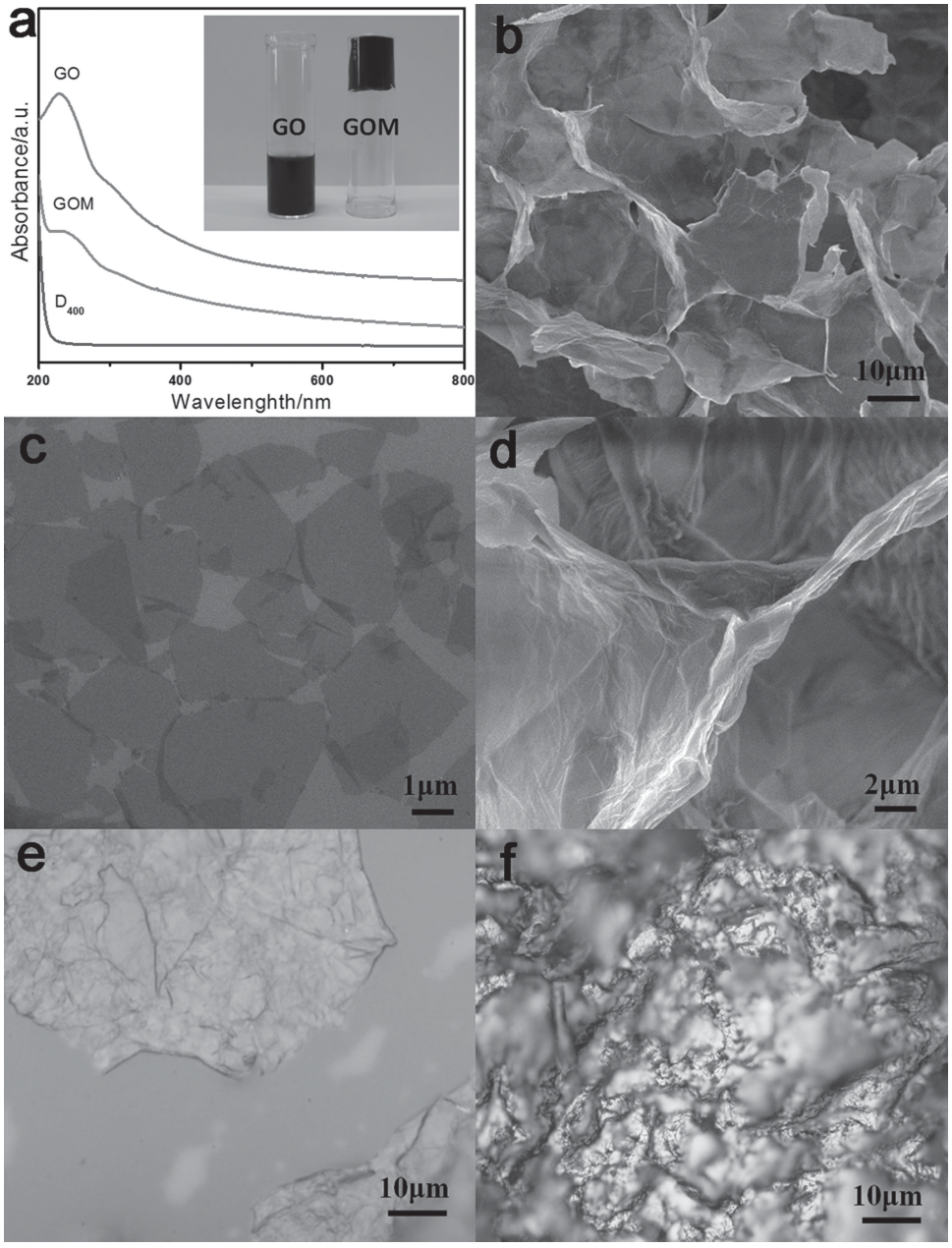

Figure 1. a) UV-vis spectra of D_{400}, GO, and GOM, insert digital photograph shows pure GO (left) and thermally cross-linked GOM by D_{400} (right). b,c) SEM images of GOM and GO, respectively. d) Enlarged SEM image of (b). e,f) Optical microscope images of GO and GOM, respectively.

2. Results and Discussion

2.1. Ultrafast Fabrication of Covalently Cross-linked GOM

From a chemical point of view, GO can be viewed as a macropolymer that is decorated by a large number of highly reactive oxygen-containing functional groups, such as carboxylic groups at the edge or epoxy and hydroxyl groups located on the basal planes (Scheme S1).[27] In polymer chemistry, the ring opening reaction of epoxy groups is an effective chain growth polymerization method to prepare specific polymers.[28] In our study, the epoxy groups on the surface of GO were employed as the reactive sites to react with epoxy curing agent D_{400}. This ultrafast cross-linking reaction can form GOM in just 1 min at 90 °C (Video-S1). In a control experiment, pure GO was heated without D_{400}, and no monolith was formed. There was no change in the color or morphology of the GO dispersion and the corresponding UV-vis absorption peak maximum remained at 230 nm, the same as untreated GO (**Figure 1**a), showing neither cross-linking nor reduction. Therefore, D_{400} is a critical component in the ultrafast formation of GOMs. Previously, the reaction between D_{400} and GO was used in the preparation of GO/polyimide composite films, but no monolith was formed when the reaction was conducted in dimethylacetamide (DMAc).[29] We also observed no monolith formation when GO and D_{400} were heated in DMAc (Figure S1a). However, when the GO/D_{400} mixture received a heat treatment in a DMAc/water mixture, a cross-linked monolith was formed (Figure S1b), indicating that an aqueous environment is essential for successful monolith formation. Scanning electron microscope (SEM) images reveal that the monolithic structure consists of macroporous building blocks which were constructed from intercalated GO sheets stacked together (Figure 1b,d). Figure 1c shows an SEM image of the uncross-linked flat GO sheets that are attached to the surface of a Si wafer. From the SEM image it can be seen that the size of the building blocks of the GOM is on the order of tens of micrometres in diameter, which is within the visible range of an optical microscope. Figure 1e is an optical microscope image of flat GO sheets that are attached to the surface of a glass slide. However, the optical microscope image of GOM shows that the gross morphology significantly changes to a rough surface consisting of peaks and valleys after cross-linking (Figure 1f). The transformation from 2D GO sheets to a 3D intercalated structure was further evidenced by the unfocused areas of the GOM image, due to the narrow focal plane of the optical microscope. Optical profilometry measurements also revealed that the surface of the GOM was considerably rough with an amplitude parameter (Sa) of 39 µm (**Figure 2**). This value was consistent with the SEM observations that the macropores of the GOM were between 30–40 µm.

The cross-linking reaction takes place very quickly with D_{400}. We propose that the driving force for the formation of GOM is the ring opening reaction between epoxy and amine groups (Scheme S1). Fourier transform infrared spectroscopy (FTIR) analysis shows the appearance of two new peaks at 1260 and 796 cm^{-1} after the reaction (**Figure 3**a), consistent with the formation of new C–N bonds (a detailed comparison of the FTIR spectra is given in the Supporting Information, Figure S2). For comparison, in a control experiment, when GO was mixed with D_{400} without heat treatment, the mixture did not form GOM after one month at room temperature and the FTIR spectrum of the sample revealed no C–N peaks (Figure S3), indicating that no significant reaction occurs at room temperature. The formation of C–N covalent bonds in the GOM structure was further confirmed by X-ray photoelectron sectroscopy (XPS) analysis. Figure 3b shows that both GO and GOM have C1s and O1s peaks in the survey spectrum, while the XPS survey spectrum of GOM shows a new distinct N1s peak at the binding energy about 400 eV, which is consistent with the formation of a C–N bond. In addition, it was also found that no monolith was formed when GO was reacted with methyl iodide quaternized D_{400} (Figure S4 and S5), indicating that covalent bonds, rather than electrostatic interactions, dominates the monolith formation mechanism.

2.2. Three Different Conformations

GOM could be formed within 1 min when the weight ratio of D_{400} to GO was within the range 0.5–8. Under other ratios, the resultant products remained yellow brown solutions and no monolith was formed. We found that the intercalations of

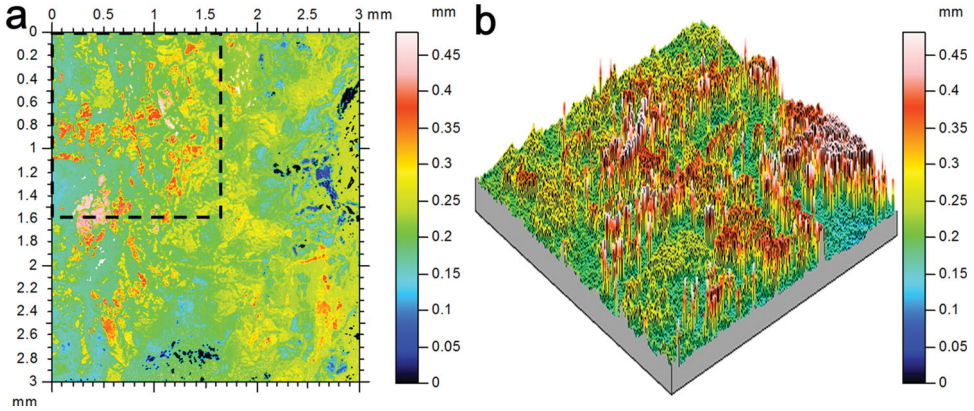

Figure 2. a) Surface roughness of the GOM measured by profile meter (3 mm × 3 mm area). b) Corresponding 3D view of the marked area in (a).

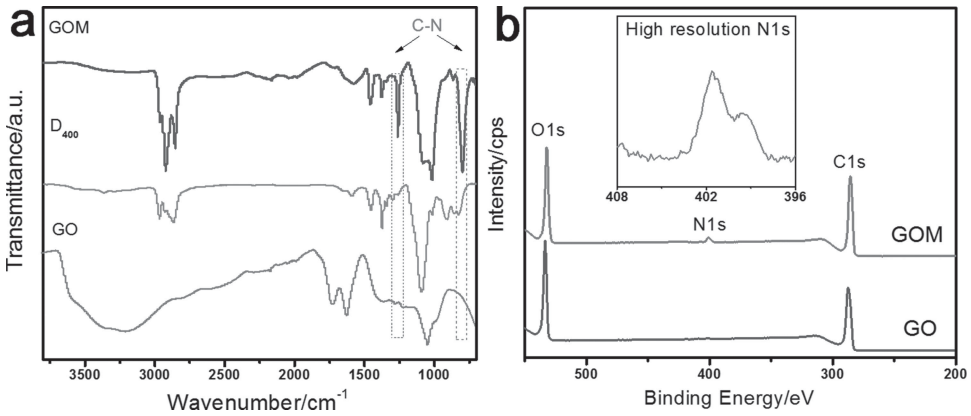

Figure 3. a) FTIR of GO, D_{400} and GOM; b) XPS spectra of GO and GOM.

linear diamines with GO may result in three different geometries depending on the amount of D_{400} employed in the reaction (**Figure 4**), i.e., (a) a loop conformation, where both ends of the diamines react with epoxy groups located in the same GO sheet; (b) a bridge conformation, where each end of the D_{400} reacts with epoxy groups located in different GO sheets, and; (c) a tail conformation, where only one end of the diamines reacts with one epoxy group in a GO sheet, leaving another amine unreacted. Robert et al. were first to propose the possibility of the existence of these three different conformations when graphene oxide sheets are intercalated by diaminoalkanes.[30] However, no evidence was given or has since been given to support this hypothesis. Moreover, Robert et al. did not report the formation of monolithic structures in their work.

In our study, we demonstrate that three different products could result from the reaction of GO with D_{400}, as demonstrated by the radically different mechanical properties measured by rheometer. As shown in **Figure 5**, the storage modulus of the product dramatically varies depending on the ratio of D_{400} used in the reaction. At a low D_{400} concentration, the product mainly contains the loop conformation (e.g., ratios <0.02), while at a high concentration the tail conformation predominates (e.g., ratios >50). As illustrated in Figure 4, these two conformations cannot result in a cross-linked structure; instead, the GO sheets exist as individual separated plates in solution even after a very long reaction time (Figure S6). As a result, the storage moduli in these cases were lower than 100 Pa (Figure 5a). Moreover, the modulus of the tail conformation product was significant lower than the original GO solution, presumably due to the formation of PPOylated GO structure. We found that the cross-linked GOM can only be formed under certain conditions (limited reaction ratios) where D_{400} molecules can form bridges between the GO sheets. The inset picture in Figure 5a shows that a stable GOM was synthesized when the weight ratio of D_{400}/GO was 2, resulting in a much higher storage modulus compared to other ratios.

From the proposed schematic illustration (Figure 4), the interlayer distance may be different in different conformations. For example, the loop conformation is expected to have the smallest d spacing as both ends of the D_{400} react with the same GO surface, whilst the tail conformation may result in the largest interlayer space, as only one end of the diamine reacts with GO and the molecular chain of D_{400} is in the extended conformation. While, theoretically, the formation of all three conformations would be expected in the reaction mixture, the GO-to-diamine molar ratio can influence the relative proportion of the resulting conformations formed. X-ray diffraction (XRD) patterns confirmed that the d spacing of the products varied dramatically when different amounts of D_{400} were employed to react with GO. For pure GO, the d spacing was about 0.79 nm. However, a new peak at $2\theta = 10.5°$ appears when a small amount of D_{400} (D_{400}/GO = 0.02) is added, corresponding to an interlayer spacing of 0.84 nm. Meanwhile, the presence of a d = 0.72 nm peak indicated the co-existence of some free GO sheets. The bridge conformation resulted in a single peak with

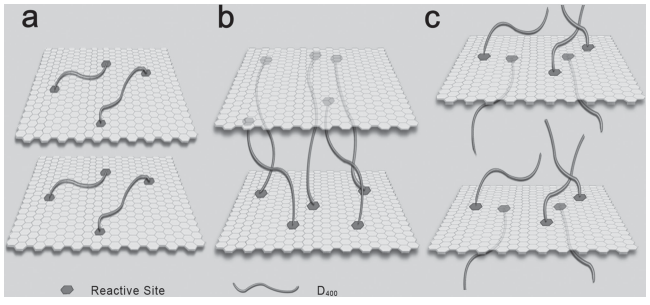

Figure 4. Proposed schematic illustration of the three different geometries that are formed under different ratio of D_{400} to GO: a) loop conformation, b) bridge conformation, c) tail conformation.

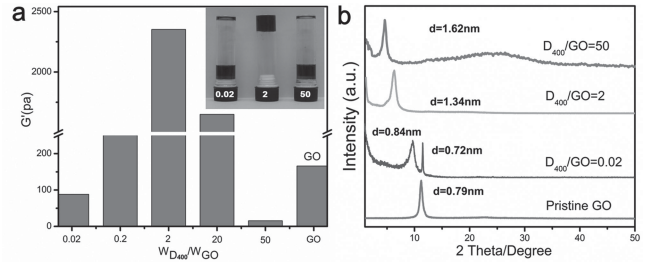

Figure 5. a) Rheological measurement of GOM products prepared under different weight ratios of D_{400} to GO. b) Corresponding XRD patterns of pure GO and GO intercalated with different amounts of D_{400}.

a d spacing of 1.34 nm, while the existence of a tail conformation was reflected by a new peak at $2\theta = 5.4°$, corresponding to an interlayer spacing of 1.62 nm. There was also a new broad peak at about 26°, corresponding to the reduced graphene oxide peak. This finding is consistent with our previous work, suggesting that GO can be partially reduced by diamines.[31]

The cross-linking reaction was simulated by molecular dynamics (MD) modeling (**Figure 6**a) to confirm our experimental findings. Figure 6b shows the plot of the distance between model GO sheets versus time for a molecular dynamics calculation of two model GO sheets linked by three D_{400} molecules (bridge conformation). The equilibrium distance of the bridge conformation was calculated to be around 14–15 Å, which is in good agreement with the experimental results (13.4 Å) obtained from the XRD patterns. The loop and tail structures were also simulated using the same MD protocol. In both cases, there was no interaction between functionalized GO sheets and the individual sheets drifted apart during the simulation. These results were consistent with our experimental observations that these adducts only resulted in homogeneous dispersions (Figure S6). Given that the zeta potentials for these loop and tail adducts were –31 mV and –21 mV, respectively, there would be strong electrostatic repulsion between the untethered GO sheets and it would be reasonable that these would exist as individual sheets in water.

2.3. Formation of GOM by Diamines with Different Chain Lengths

In addition to D_{400}, a series of diamines with different chain lengths (from D_{88} to D_{2000}, their structures are listed in Table S1) were investigated to elucidate the effect of chain length on cross-linking reaction between GO and diamines. These other diamines were able to form GOMs, but usually required a longer reaction time (>1 min). Rheological measurements of these GO/diamine systems demonstrated that the moduli of the products were not as high as that of D_{400} under the same reaction conditions (Figure S7), showing that D_{400} was the best diamine cross-linker to fabricate GOM among the diamines tested. In addition, XRD analysis showed that the interlayer spacing of the product varied as GO reacted with diamines of different chain lengths (**Figure 7**). Therefore, the

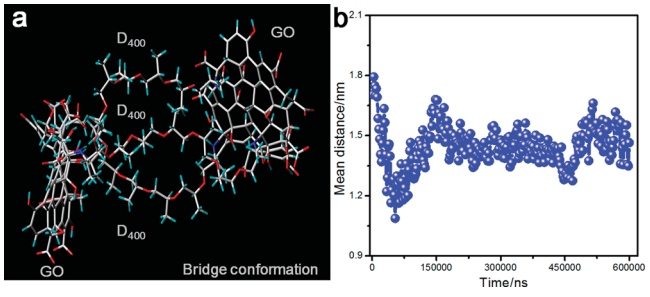

Figure 6. a) Molecular dynamics modeling of two GO sheets linked by three D_{400} molecules. b) Plot of the distance between model GO sheets versus time for the bridge conformation.

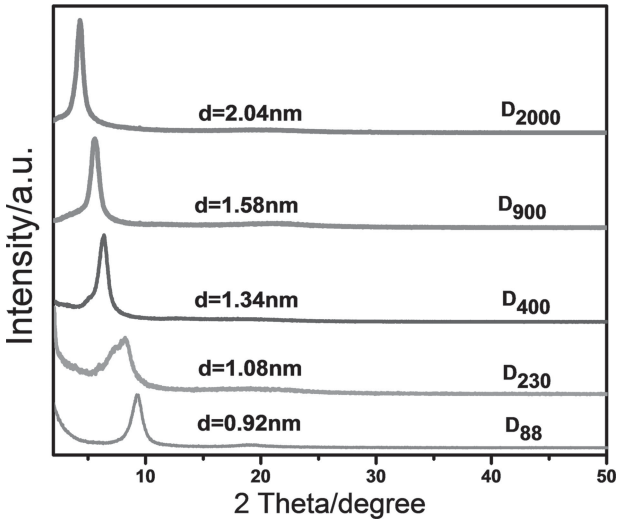

Figure 7. XRD patterns of GO intercalated by diamines of different chain length (diamine/GO weight ratio is 2 for all the samples).

interlayer spacing of GO sheets can be tuned by changing both diamine concentration and chain length.

2.4. Multifunctional GOM

Stability tests showed that the synthesized GOM was stable under harsh conditions. Figure S8 shows the digital pictures of GOMs that were able to maintain their original shape and integrity after immersion in strong acid (pH = 1) and base (pH = 13) solutions for 2 months. The prepared GOM was found to behave like an elastic hydrogel, in which dehydration and hydration can switch very quickly, triggered by water. As shown in Video-S2, the volume of the formed GOM decreased dramatically when water was absorbed by a tissue (shrunk to 22% of the original height). This conformation change was reversible when water was added again. It was found that the GOM could recover to the original shape and volume (swelled to 98% of the original height) once it was re-hydrated. Based on this conditional recovery property, the as prepared GOM served as a nanofilter readily filtering a model eluent, methylene blue, from aqueous solution with an adsorption capacity of 465 mg/g (Figure S9).

Carbon nanomaterials have shown great potential in various biomedical applications such as drug delivery, bioimaging, and biosensing.[32] However, the bioapplications of the newly developed 3D graphene monolithic structure has been limited. Our as-prepared GOM offers a potential scaffold for tissue engineering owing to its highly interconnective porous structure. Initial cytotoxicity assessment of the GOM was performed by culturing of the human fibroblast cell line (L929) on the surface of GOM. Within 24 h, most of L929 cells were found to attach to the GOM scaffold (Figure S10). After 3 days, L929 cells proliferated, migrated along the skeleton of GOM and grew in a 3D fashion (**Figure 8**a). Moreover, the presence of unfocused cells suggests that the L929 cells have migrated into the GOM porous structure. The cell viability reached 99% and 93% after

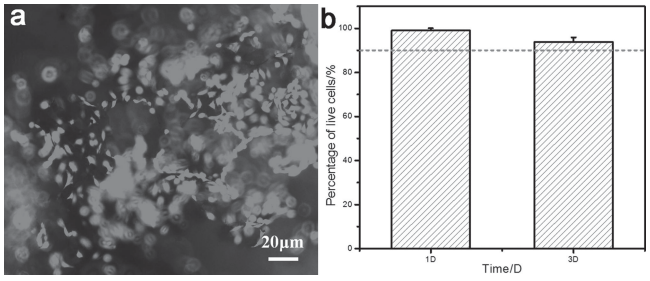

Figure 8. L929 adhesion and proliferation on GOM. (a) Cell viability assay of L929 cells on GOM after 72 h of culture as determined by live/dead assay, live cells were stained green and dead cells were stained red. (b) The percentage of live cells on GOM after 1 day and 3 days of culture.

24 and 72 h respectively, (Figure 8b), showing non-cytotoxicity, consistent with reported 3D graphene foams[33] and 2D graphene film.[34] Thus, GOM provides a good substrate for the adhesion and proliferation of L929 cells, suggesting that our GOM scaffold may have potential for use in biomedical applications.

In comparison to previously reported methods of fabricating graphene based macroassemblies, the cross-linking methodology developed in this study has the advantage of simplicity, scalability, and rapid fabrication. This thermal cross-linking method involving D_{400} can fabricate GOMs in arbitrary moulds simply by heating. Video S3 demonstrates the formation of GOM in a glass bottle in about 10 s using a heating gun. In addition, the fast cross-linking method has provided an alternative way to fabricate graphene monolithic structure. We found that the GOM can be readily transformed into graphene monolith (Figure S11) just by heating at 600 °C for 20 min. XPS of the carbonized GOM revealed that most of the oxygen-containing groups are removed from the GOM, while the N content did not significantly change (Table S2), consistent with our proposed mechanism that GOM is formed by covalent C–N bonds. Furthermore, the deconvoluted N1s spectrum demonstrated that the functionalized N species (NH_2/NH_3^+–C and N–C species) on the surface of GOM can be readily incorporated within the graphene lattice after annealing (Figure S12). Therefore, the cross-linking method developed in this study also provided a facile strategy to produce N-doped graphene macrostructures.

3. Conclusions

We have demonstrated a simple but rapid and effective method to fabricate macroassembled graphene oxide monolith (GOM) with tunable intercalation distance using commercial diamines as cross-linkers. The ring opening reaction between GO epoxides and diamines generated covalent C–N bonds which were attributed to the formation of this stable GOM, in which the GO nanosheets are stitched together by C–N bonds. It was proven that the intercalation of GO with linear diamine molecules can form three different geometries, which can result in totally different assemblies of GO. Moreover, the interlayer space of GO sheets can be controlled from 0.84 nm to 2.04 nm by intercalation with diamines of different concentrations and chain lengths. The resulting monoliths showed potential in nanofiltration and tissue engineering applications and were readily converted to graphene monoliths by thermal treatment. Our findings have provided new insights into the reaction mechanism of covalently cross-linked GOM structures, which may facilitate the rational design and versatile production of graphene based materials.

4. Experimental Section

Fabrication of GOM: Graphene oxide (600 mesh) was initially prepared by the modified Hummers method.[35] Typically, GOM was fabricated by heating a mixture of D_{400} (Huntsman Corporation Australia Pty Ltd, 12 mg) with GO solution (2 mL, 3 mg/mL in water) at 90 °C for 1 min (See supporting information Video-S1). Note that the ultrafast formation of GOM can only occur in water dispersion. Dehydrated GOMs were obtained by freeze drying of the as-synthesized monoliths. A range of diamines were investigated in the formation of GOMs. All ratios mentioned in this work are weight ratios. Quaternized D_{400} was prepared by adding D_{400} (2.382 g) dropwise to vigorously stirred methyl iodide (11.400 g) at room temperature. After 15 min, the reaction mixture was dried under vacuum at 70 °C for 24 h to afford a viscous liquid.

Molecular Dynamics Calculations: Molecular dynamics (MD) calculations of a model GOM were carried out using Sybylx2.0 on an i7 processor running RedHat linux. Calculations used a model for GO (Figure 6) based on that by R.S. Ruoff.[36] Three D_{400} linkers were added at the appropriately spaced attachment points. The structures were annealed for 100 ps and simulated for 600 ns until it was clear that an equilibrium distance between the GO sheets had been reached. The Merck Molecular Force Field (MMFF) and partial atomic charges, and implicit solvent (dielectric constant of 80) were used.

Cytotoxicity Assay: GOM samples were placed into wells of a 96-well polystyrene cell culture plate and soaked overnight in two changes of culture media, then rinsed with phosphate buffer solution (PBS) to remove soluble impurities. The samples were sterilized by rinsing with 75% ethanol then placed under UV light for 20 min in a laminar flow hood. Samples were seeded with 5×10^3 L929 human fibroblast cells per well, and cultured in MEM-GlutaMax nutrient mixture (Life Technologies, USA), supplemented with 10% Fetal Bovine Serum (Life Technologies, USA) at 37 °C in 5% CO_2, 1% Anti-Anti (Antibiotic, antimycotic, Life Technologies, USA), and 1% NEAA (Life Technologies, USA). After 24 h and 72 h, the cells were stained with Calcein AM, which is cleaved to yield a green fluorescent product by metabolically active cells and red fluorescent product by dead cells. Images were obtained using a Nikon TE 2000-U microscope and analyzed by Image J software.

Characterization: The morphology and structure of GOMs were examined by field emission scanning electron microscopy (FE-SEM Philips XL30). The surface morphology of the GOM was analyzed with Altimet Altisurf 500 (Cotec) optical profilometer. UV-Vis absorption spectra were recorded on an Agilent HP 8453 UV-Vis spectrophotometer. Optical images were obtained with an Olympus GX71 optical microscope. ^{1}H NMR spectroscopy was conducted on a 400 MHz Bruker Ultrashiled Spectrometer (Bruker, Germany) in MeOD. The Fourier transform-infrared (FTIR) spectrum was recorded with Thermo Nicolet 6700 FTIR Spectrometer. A Bruker D8 Advance X-ray Diffractometer using Cu$K\alpha$ radiation (40 kV, 40 mA) equipped with a LynxEye silicon strip detector was employed to obtain the XRD patterns. X-ray photoelectron spectroscopy (XPS) characterizations were performed in an AXIS Ultra-DLD spectrometer (Kratos Analytical Ltd. Manchester) equipped with a monochromated Al Kα X-ray source. The dynamic rheological measurements of the products were performed on an ARES rheometer (TA Instruments, USA), the storage modulus (G′) were collected under 90 °C for 1 min.

Supporting Information

Supporting Information is available from the Wiley Online Library or from the author.

Acknowledgements

This work was partly supported by NSFC (Nos. 51072028, 21361162004, and 21336001), China Scholarship Council (CSC), and the Program for Zhejiang Leading Team of Science and Technology Innovation (No. 2009R50039). The authors acknowledge K. Hands and M. Greaves (CMSE, Clayton) for SEM and optical profilometry measurements. The authors are thankful to Dr T. Gengenbach (CMSE, Clayton) for assistance with the XPS characterization. The authors would like to thank Drs M. Gao and L. Randeniya (CSIRO) for helpful discussions regarding the manuscript.

Received: November 11, 2013
Revised: February 17, 2014
Published online: April 23, 2014

[1] K. S. Novoselov, A. K. Geim, S. V. Morozov, D. Jiang, Y. Zhang, S. V. Dubonos, I. V. Grigorieva, A. A. Firsov, *Science* **2004**, *306*, 666.
[2] K. S. Kim, Y. Zhao, H. Jang, S. Y. Lee, J. M. Kim, K. S. Kim, J. H. Ahn, P. Kim, J. Y. Choi, B. H. Hong, *Nature* **2009**, *457*, 706.
[3] D. R. Dreyer, H. P. Jia, C. W. Bielawski, *Angew. Chem. Int. Ed.* **2010**, *49*, 6813.
[4] X. Yang, J. Zhu, L. Qiu, D. Li, *Adv. Mater.* **2011**, *23*, 2833.
[5] Z. Tang, S. Shen, J. Zhuang, X. Wang, *Angew. Chem. Int. Ed.* **2010**, *49*, 4603.
[6] D. Li, M. B. Muller, S. Gilje, R. B. Kaner, G. G. Wallace, *Nat. Nanotechnol.* **2008**, *3*, 101.
[7] D. A. Dikin, S. Stankovich, E. J. Zimney, R. D. Piner, G. H. B. Dommett, G. Evmenenko, S. T. Nguyen, R. S. Ruoff, *Nature* **2007**, *448*, 457.
[8] D. W. Wang, F. Li, J. Zhao, W. Ren, Z. G. Chen, J. Tan, Z. S. Wu, I. Gentle, G. Q. Lu, H. M. Cheng, *ACS Nano* **2009**, *3*, 1745.
[9] S. Bae, H. Kim, Y. Lee, X. Xu, J. S. Park, Y. Zheng, J. Balakrishnan, T. Lei, H. Ri Kim, Y. I. Song, Y. J. Kim, K. S. Kim, B. Ozyilmaz, J. H. Ahn, B. H. Hong, S. Iijima, *Nat. Nanotechnol.* **2010**, *5*, 574.
[10] J. T. Robinson, F. K. Perkins, E. S. Snow, Z. Wei, P. E. Sheehan, *Nano Lett.* **2008**, *8*, 3137.
[11] L. K. Randeniya, H. Shi, A. S. Barnard, J. Fang, P. J. Martin, K. Ostrikov, *Small* **2013**, 3993.
[12] Y. Zhao, C. Hu, Y. Hu, H. Cheng, G. Shi, L. Qu, A Versatile, *Angew. Chem. Int. Ed.* **2012**, *51*, 11371.
[13] M. A. Worsley, P. J. Pauzauskie, T. Y. Olson, J. Biener, J. H. Satcher, T. F. Baumann, *J. Am. Chem. Soc.* **2010**, *132*, 14067.
[14] L. Qiu, J. Z. Liu, S. L. Y. Chang, Y. Wu, D. Li, *Nat. Commun.* **2012**, *3*, 1241.
[15] Y. Xu, K. Sheng, C. Li, G. Shi, *ACS Nano* **2010**, *4*, 4324.
[16] Q. Wu, Y. Q. Sun, H. Bai, G. Q. Shi, *Phys. Chem. Chem. Phys.* **2011**, *13*, 11193.
[17] C. Huang, H. Bai, C. Li, G. Shi, *Chem. Commun.* **2011**, *47*, 4962.
[18] W. Lv, Y. Tao, W. Ni, Z. Zhou, F. Y. Su, X. C. Chen, F. M. Jin, Q. H. Yang, *J. Mater. Chem.* **2011**, *21*, 12352.
[19] X. Jiang, Y. Ma, J. Li, Q. Fan, W. Huang, *J. Phys. Chem. C* **2010**, *114*, 22462.
[20] H. Bai, C. Li, X. L. Wang, G. Q. Shi, *Chem. Commun.* **2010**, *46*, 2376.
[21] H. Bai, C. Li, X. Wang, G. Shi, *J. Phys. Chem. C* **2011**, *115*, 5545.
[22] W. F. Chen, L. F. Yan, *Nanoscale* **2011**, *3*, 3132.
[23] H. Bai, K. Sheng, P. Zhang, C. Li, G. Shi, *J. Mater. Chem.* **2011**, *21*, 18653.
[24] Y. Xu, Q. Wu, Y. Sun, H. Bai, G. Shi, *ACS Nano* **2010**, *4*, 7358.
[25] P. M. Sudeep, T. N. Narayanan, A. Ganesan, M. M. Shaijumon, H. Yang, S. Ozden, P. K. Patra, M. Pasquali, R. Vajtai, S. Ganguli, A. K. Roy, M. R. Anantharaman, P. M. Ajayan, *ACS Nano* **2013**, *7*, 7034.
[26] Z. Y Sui, Y Cui, J. H Zhu, B. H Han, *ACS Appl. Mater. Interfaces* **2013**, *5*, 9172.
[27] C. W. Bielawski, D. R. Dreyer, S. Park, R. S. Ruoff, *Chem. Soc. Rev.* **2010**, *39*, 228.
[28] R. E. Parker, N. S. Isaacs, *Chem. Rev.* **1959**, *59*, 737.
[29] W. H. Liao, S. Y. Yang, J. Y. Wang, H. W. Tien, S. T. Hsiao, Y. S. Wang, S. M. Li, C. C. Ma, Y. F. Wu, *ACS Appl. Mater. Interfaces* **2013**, *5*, 869.
[30] G. Zhou, L. C. Yin, D. W. Wang, L. Li, S. Pei, I. R. Gentle, F. Li, H. M. Cheng, *ACS Nano* **2013**, *7*, 5367.
[31] H. Hu, Z. Zhao, W. Wan, Y. Gogotsi, J. Qiu, *Adv. Mater.* **2013**, *25*, 2219.
[32] C. Chung, Y. K. Kim, D. Shin, S. R. Ryoo, B. H. Hong, D. H. Min, *Acc. Chem. Res.* **2013**, *46*, 2211.
[33] N. Li, Q. Zhang, S. Gao, Q. Song, R. Huang, L. Wang, L. Liu, J. Dai, M. Tang, G. Cheng, *Sci. Rep.* **2013**, *3*, 1640.
[34] H. Chen, M. B. Müller, K. J. Gilmore, G. G. Wallace, D. Li, *Adv. Mater.* **2008**, *20*, 3557.
[35] W. S. Hummers, R. E. Offeman, *J. Am. Chem. Soc.* **1958**, *80*, 1339.
[36] S. Park, R. S. Ruoff, *Nat. Nanotechnol.* **2009**, *4*, 217.